nature catalysis

Supplementary information

https://doi.org/10.1038/s41929-024-01219-z

# Unveiling metal mobility in a liquid Cu–Ga catalyst for ammonia synthesis

In the format provided by the authors and unedited

# Table of Contents

**Supplementary Fig. 1.** Phase diagram of the Cu-Ga binary alloy, covering the composition range 0 – 100 at.% Ga. Figure adapted with permission.[1] ..... 3
**Supplementary Fig. 2**. (a) A bright field TEM image collected of the Cu-Ga droplet during *in-situ* heating, indicating the metal droplet exists in the liquid phase. (b) SAED of the droplet at room temperature, showcasing the crystallinity of the intermetallic core. (c) SAED of the droplet after heating, confirming the transitioning of the droplet from a crystalline to an amorphous material. ..... 4
**Supplementary Fig. 3.** The effect of Cu loading in the Cu-Ga catalyst on the ammonia production rate, obtained at 400 ºC and 4 bar. ..... 5
**Supplementary Fig. 4.** Schematic of the ammonia synthesis reaction set up, depicting the use of a liquid metal catalyst in a Harrick reactor. The reaction products are collected periodically for analysis using colorimetric methods and NMR. ..... 6
**Supplementary Fig. 5.** Comparison of ammonia concentration measurements obtained using NMR and Nessler reagent, showcasing the high comparability of the results obtained through both methods. ..... 7
**Supplementary Fig. 6.** NMR analysis of the product catalyzed using Cu-Ga, at 400 °C and 4 bar. ..... 8
**Supplementary Fig. 7.** Ion current analysis of m/z=17 performed over the Cu-Ga catalyst under the $N_2$ pretreatment at 400 ºC. ..... 9
**Supplementary Fig. 8.** Ion current analysis of m/z=17 performed over the $N_2$-pretreated Cu-Ga catalyst under $H_2$ flow at 400 ºC, showcasing the formation of ammonia. ..... 10
**Supplementary Fig. 9.** Effect of the $N_2/H_2$ feed mixture composition on the ammonia production rate at 400 ºC and 4 bar. ..... 11
**Supplementary Fig. 10.** Ammonia production rate over the Cu-Ga catalyst at different pressures, showcasing the increase in the production rate at higher pressures at 400 ºC. ..... 12
**Supplementary Fig. 11.** Ammonia production rate at different temperatures, showcasing the increase in ammonia formation over the Cu-Ga liquid metal catalyst as the reaction temperature is increased. ..... 13
**Supplementary Fig. 12.** Comparison of the ammonia production rate obtained at 400 °C and 4 bar over the Cu-Ga liquid metal catalyst, its elemental metal constituents (Cu and Ga), and the blank inert substrate. ..... 14
**Supplementary Fig. 13.** Comparison of the ammonia production rate obtained using Cu-Ga catalyst synthesized using different high-melting solvents. ..... 15
**Supplementary Fig. 14.** Cu K–edge XANES of the Cu-Ga catalyst collected at room temperature but *post reactions* at room temperature, 200 °C, 300 °C, and 400 °C. ..... 16
**Supplementary Fig. 15.** Cu K–edge EXAFS of the Cu-Ga catalyst post reaction at room temperature, 200 °C, 300 °C, and 400 °C. ..... 17
**Supplementary Fig. 16.** Cu K–edge FT of the Cu-Ga catalyst post reaction at room temperature, 200 °C, 300 °C, and 400 °C. ..... 18
**Supplementary Fig. 17.** *In-situ* DRIFTS spectra over the Cu-Ga catalyst at different reaction temperatures, whereby pure hydrogen feed was used. ..... 19
**Supplementary Fig. 18.** *In-situ* DRIFTS spectra of ammonia synthesis over pure Ga, showcasing the formation of $NH_3$ at different reaction temperatures. ..... 20

**Supplementary Fig. 19.** *In-situ* DRIFTS analysis of the Cu-Ga catalyst under $N_2$ flow at 3 bar. ..... 21
**Supplementary Fig. 20.** SEM image of the Cu-Ga catalyst after ammonia synthesis, reacted at 400 °C and 4 bar. EDX analysis (inset) was conducted as a wide area scan of the complete area encompassed in the image, showing the presence of nitrogen species post reaction. ..... 22
**Supplementary Fig. 21.** *In-situ* DRIFTS analysis of the nitrogen pretreated Cu-Ga catalyst under $H_2$ flow over time. ..... 23
**Supplementary Fig. 22.** *In-situ* DRIFTS analysis of the pure Ga catalyst under $N_2$ flow at 3 bar. ..... 24
**Supplementary Fig. 23.** *In-situ* DRIFTS analysis of the nitrogen pretreated Ga catalyst under $H_2$ flow over time. ..... 25
**Supplementary Fig. 24.** *In-situ* heating XAS experimental setup, comprising a capillary heater used to supply heat to the Cu-Ga alloys filled into 1 mm quartz capillaries. ..... 26
**Supplementary Fig. 25.** *In-situ* heating XANES spectra of the Cu-Ga alloy in quartz capillaries taken between room temperature and 675 °C, at the Cu K–edge. ..... 27
**Supplementary Fig. 26**. Cu atom pairing analysis, depicting the change in the distance between Cu atoms as a function of time in the bulk of the liquid metal from AIMD simulations at 400 °C. ..... 28
**Supplementary Fig. 27.** Atomic pairwise probability distribution in the bulk at 200 ºC from AIMD simulations. ..... 29
**Supplementary Fig. 28.** Cu atom pairing analysis, depicting the change in the distance between Cu atoms as a function of time across the liquid metal interface from AIMD simulations at 400 °C. ..... 30
**Supplementary Fig. 29.** Atomic density profiles for all atoms and for Cu atoms as a function of z-position in the interfacial system from AIMD simulations at 400 °C. ..... 31
**Supplementary Fig. 30.** AIMD simulation snapshots of each step in the catalytic reaction, with relative energies in eV. ..... 32
**Supplementary Fig. 31.** Reaction of $H_2$ with the surface in the presence and absence of Cu and N, showing relative energies in eV. ..... 33
**Supplementary Table 1.** AIMD relative energies at the different reaction steps, highlighting the difference between the Cu-Ga catalyst and pure Ga. ……34
**Supplementary Fig. 32.** NMR analysis of ammonium in control experiments when pure $N_2$ is fed into the catalytic system. Negligible ammonium peaks compared to maleic acid peaks (lower than detection limits) were observed, indicating no ammonia formation in the control experiments. ..... 35
**Supplementary Fig. 33.** FTIR spectrum of gases in the $N_2$ gas cylinder, using He gas as a blank spectrum. ..... 36
**Supplementary Fig. 34.** Detection of N (N-14), $N_2$ ($N_2$-28). NO (NO-30), and $NO_2$ ($NO_2$-46) in the reactant $N_2$ gas cylinder (>99.999%) according to mass spectroscopic responses as a function of time. The measurement is conducted with an $N_2$ flowrate of 5 ml/min. ..... 36

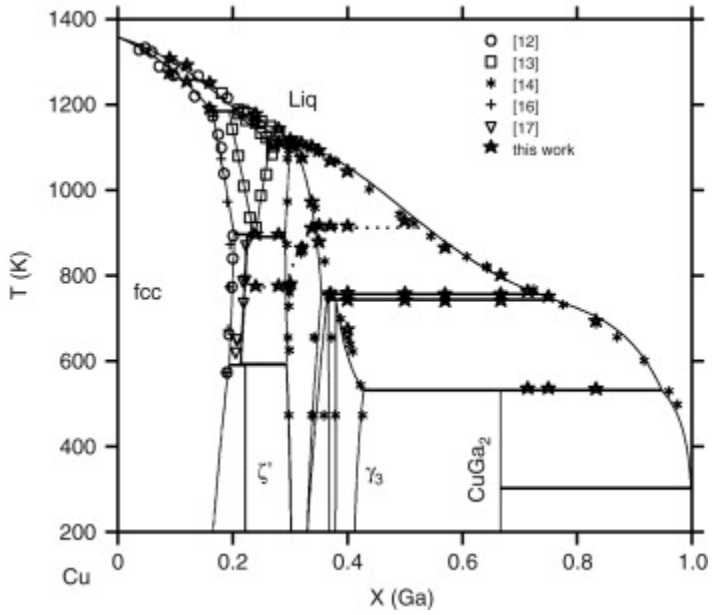


**Supplementary Fig. 1.** Phase diagram of the Cu-Ga binary alloy, covering the composition range 0 – 100 at.% Ga, showcasing the calculated phase diagram compared with experimental data. Figure adapted with permission.[1] Note that the references within the figure caption relate to the references in the cited work.

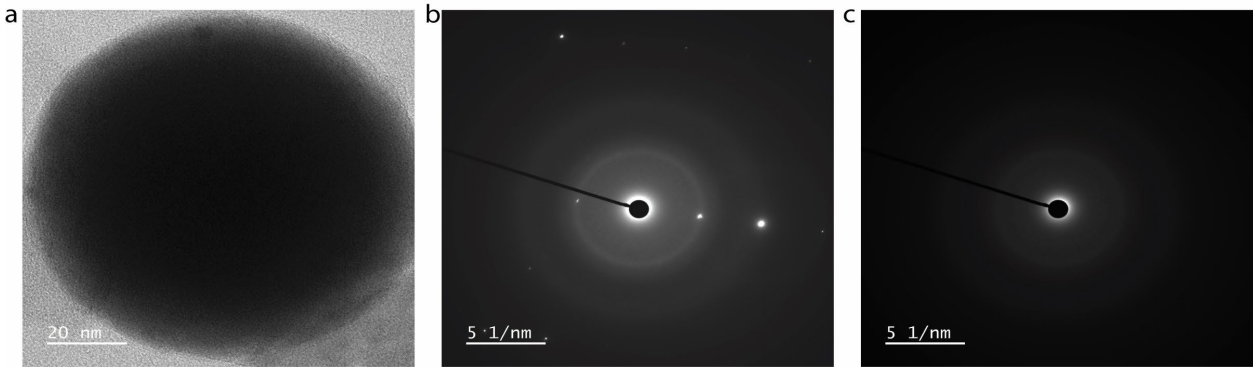


**Supplementary Fig. 2.** (a) A bright field TEM image collected of the Cu-Ga droplet during *in-situ* heating, indicating the metal droplet exists in the liquid phase. (b) SAED of the droplet at room temperature, showcasing the crystallinity of the intermetallic core. (c) SAED of the droplet after heating, confirming the transitioning of the droplet from a crystalline to an amorphous material.

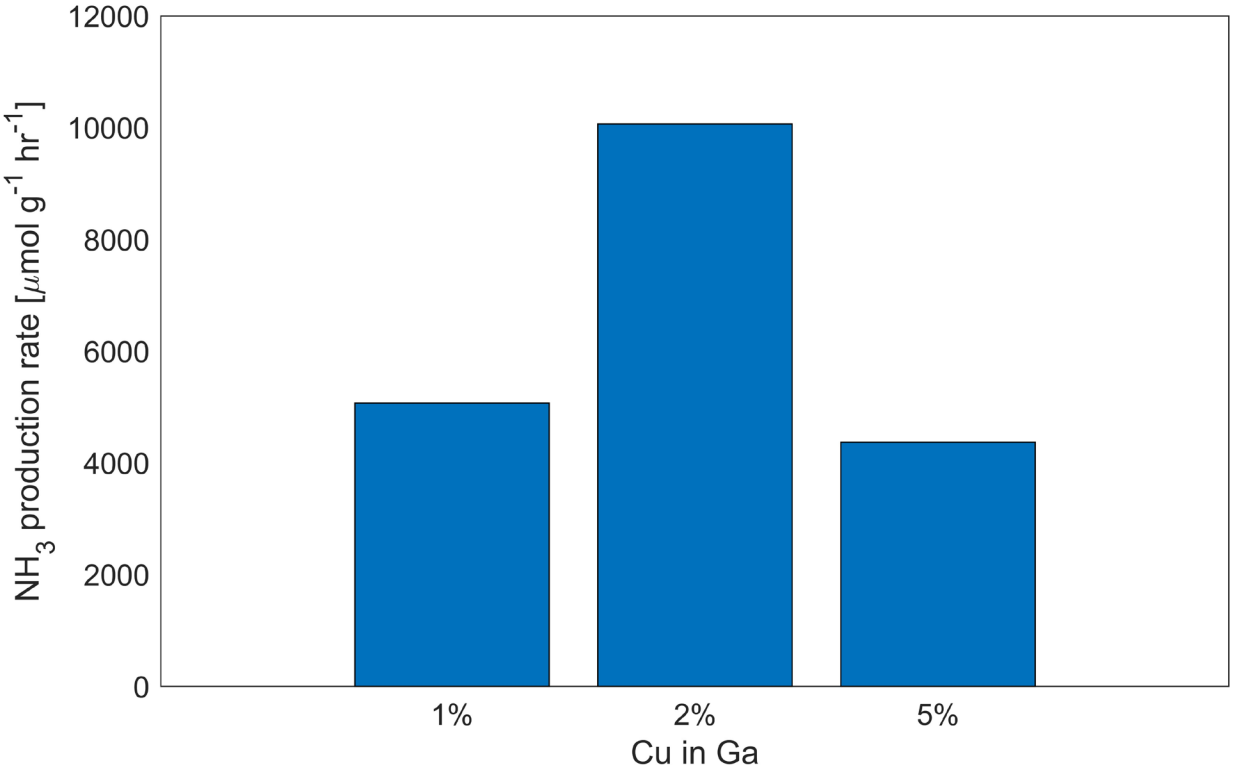


**Supplementary Fig. 3.** The effect of Cu loading in the Cu-Ga catalyst on the ammonia production rate, obtained at 400 ºC and 4 bar.

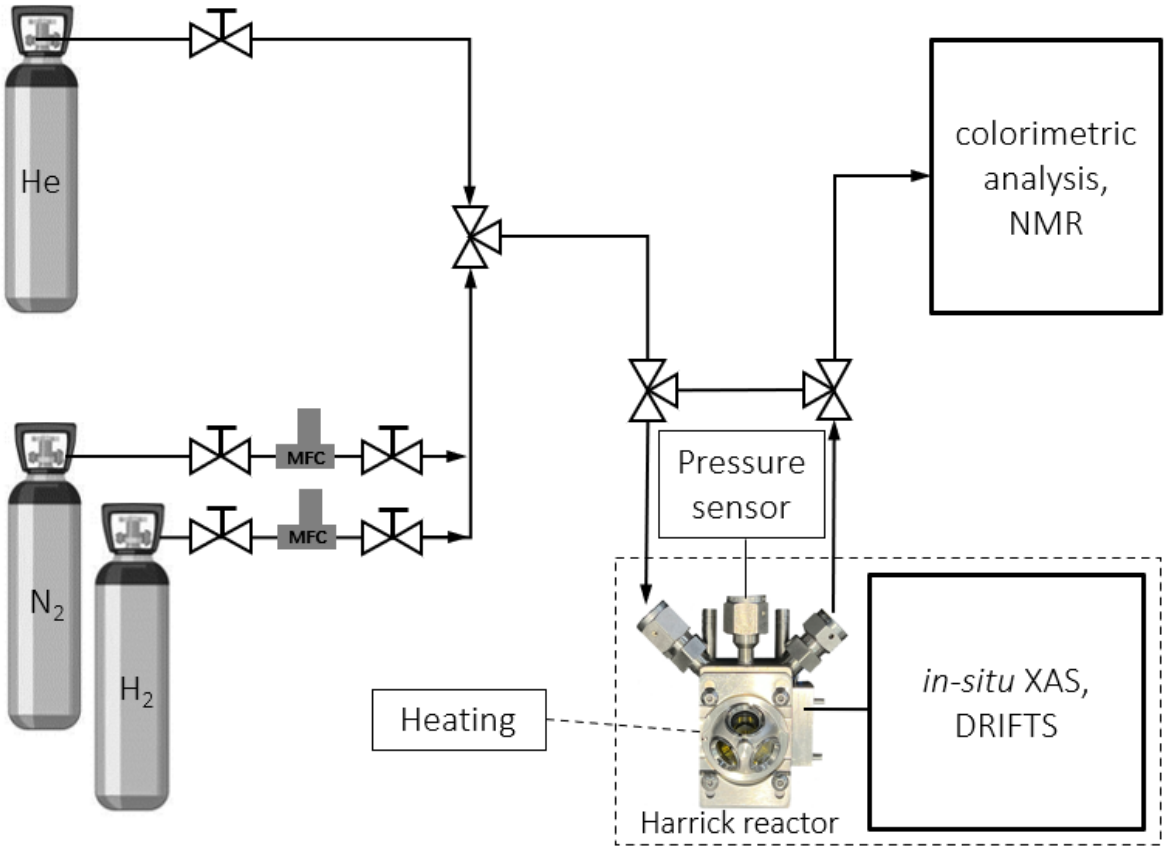


**Supplementary Fig. 4.** Schematic of the ammonia synthesis reaction set up, depicting the use of a liquid metal catalyst in a Harrick reactor. The reaction products are collected periodically for analysis using colorimetric methods and NMR.

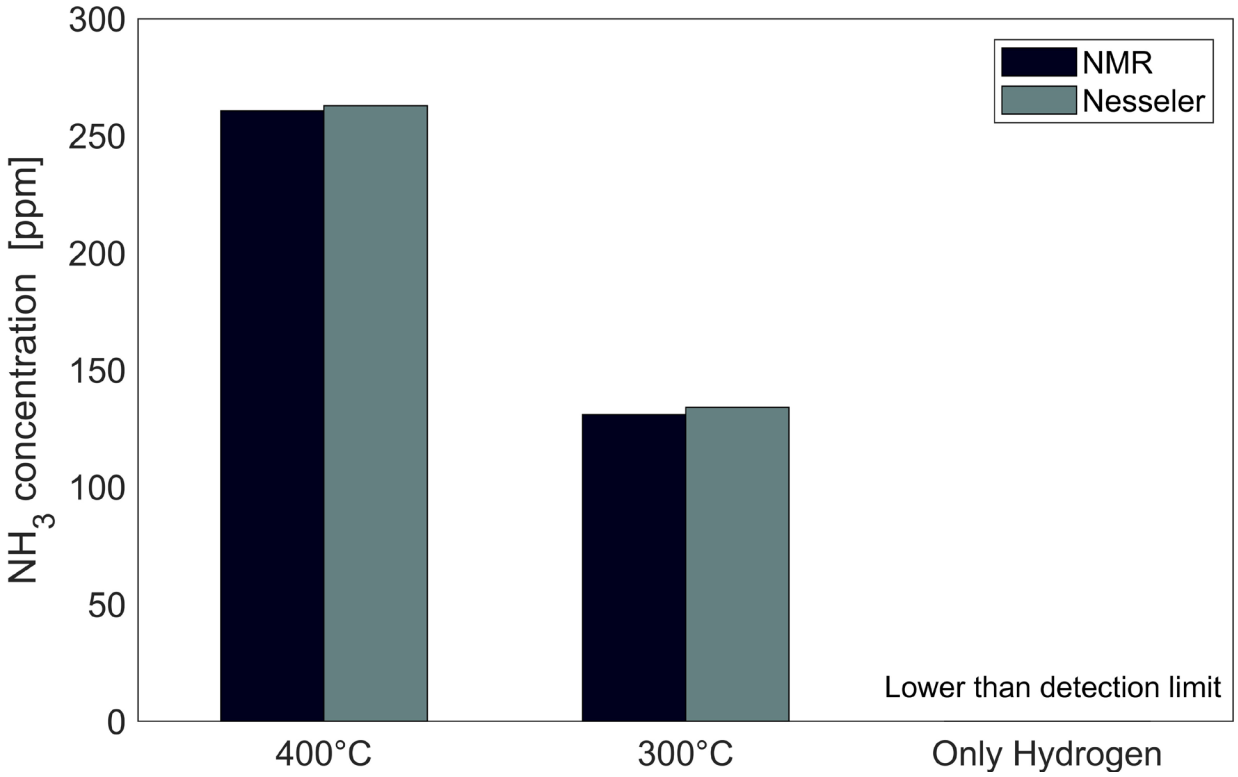


**Supplementary Fig. 5.** Comparison of ammonia concentration measurements obtained using NMR and Nessler reagent, showcasing the high comparability of the results obtained through both methods.

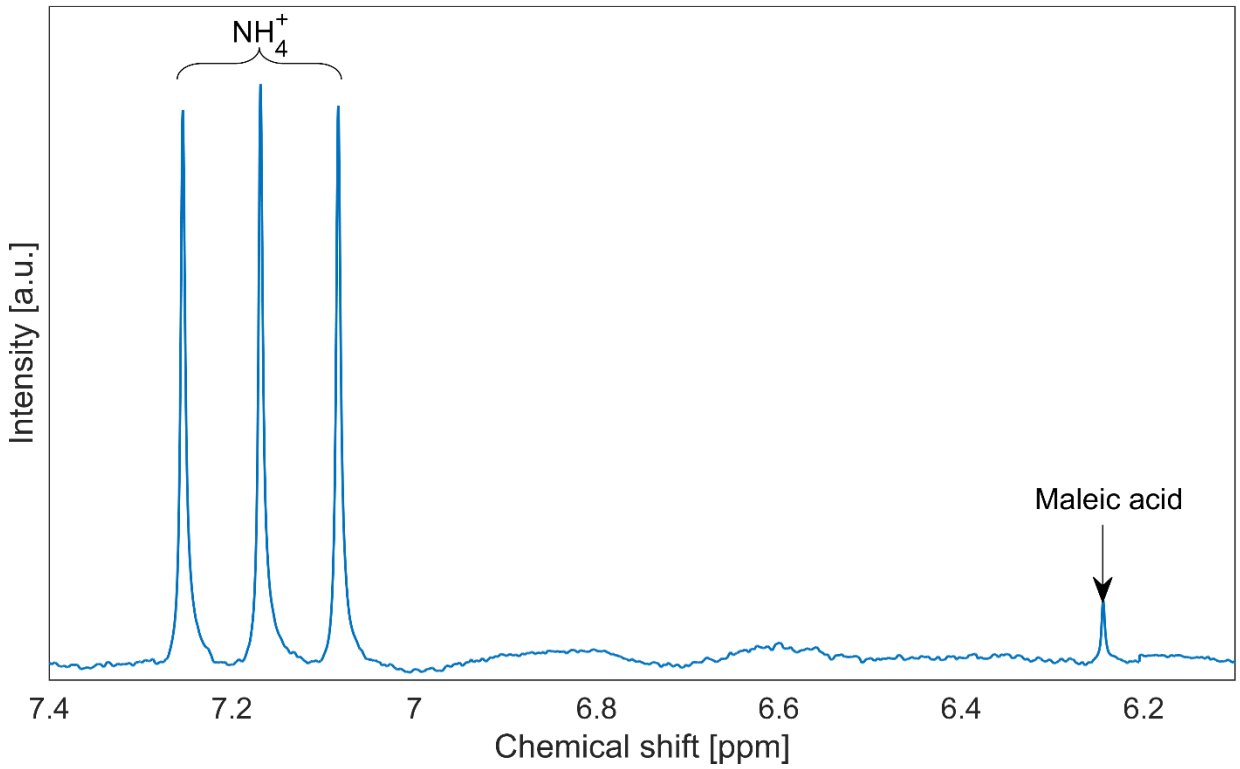


**Supplementary Fig. 6.** NMR analysis of the product catalyzed using Cu-Ga, at 400 °C and 4 bar.

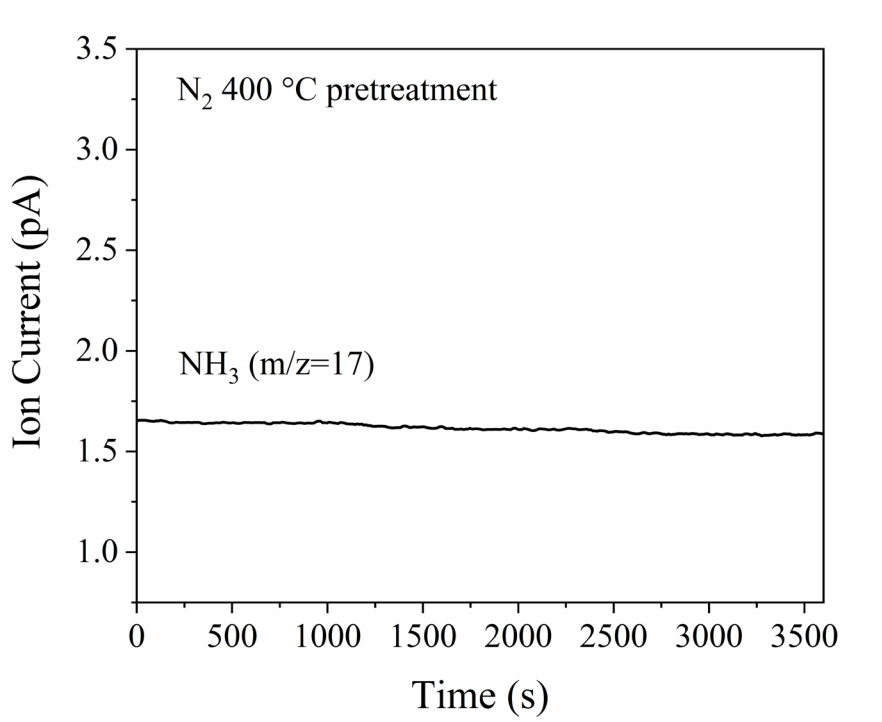


**Supplementary Fig. 7.** Ion current analysis of m/z=17 performed over the Cu-Ga catalyst under the $N_2$ pretreatment at 400 ºC.

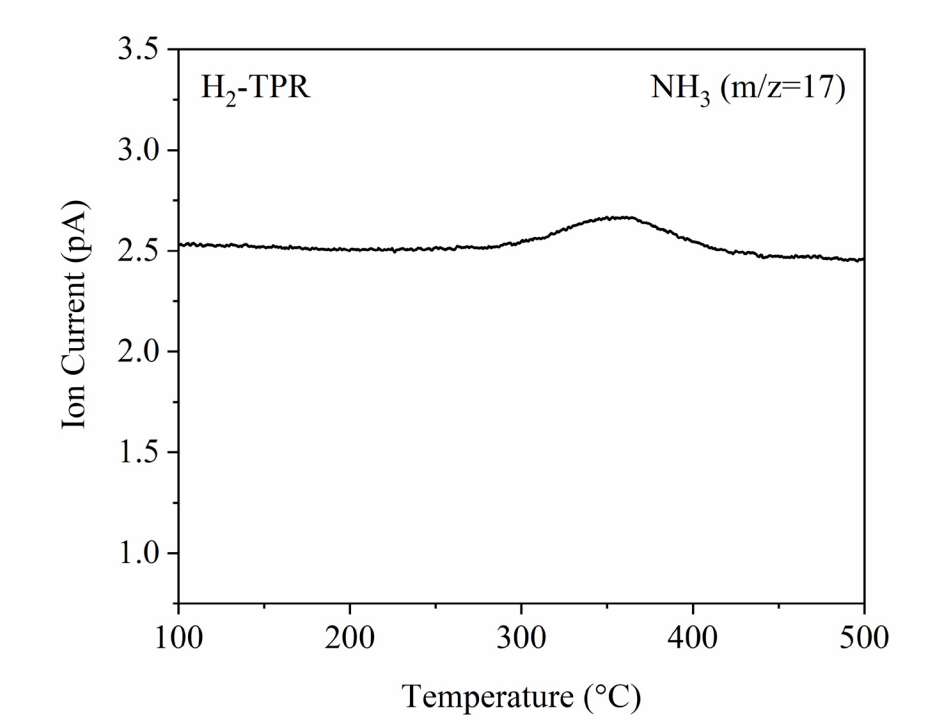


**Supplementary Fig. 8.** Ion current analysis of m/z=17 performed over the $N_2$-pretreated Cu-Ga catalyst under $H_2$ flow at 400 ºC, showcasing the formation of ammonia.

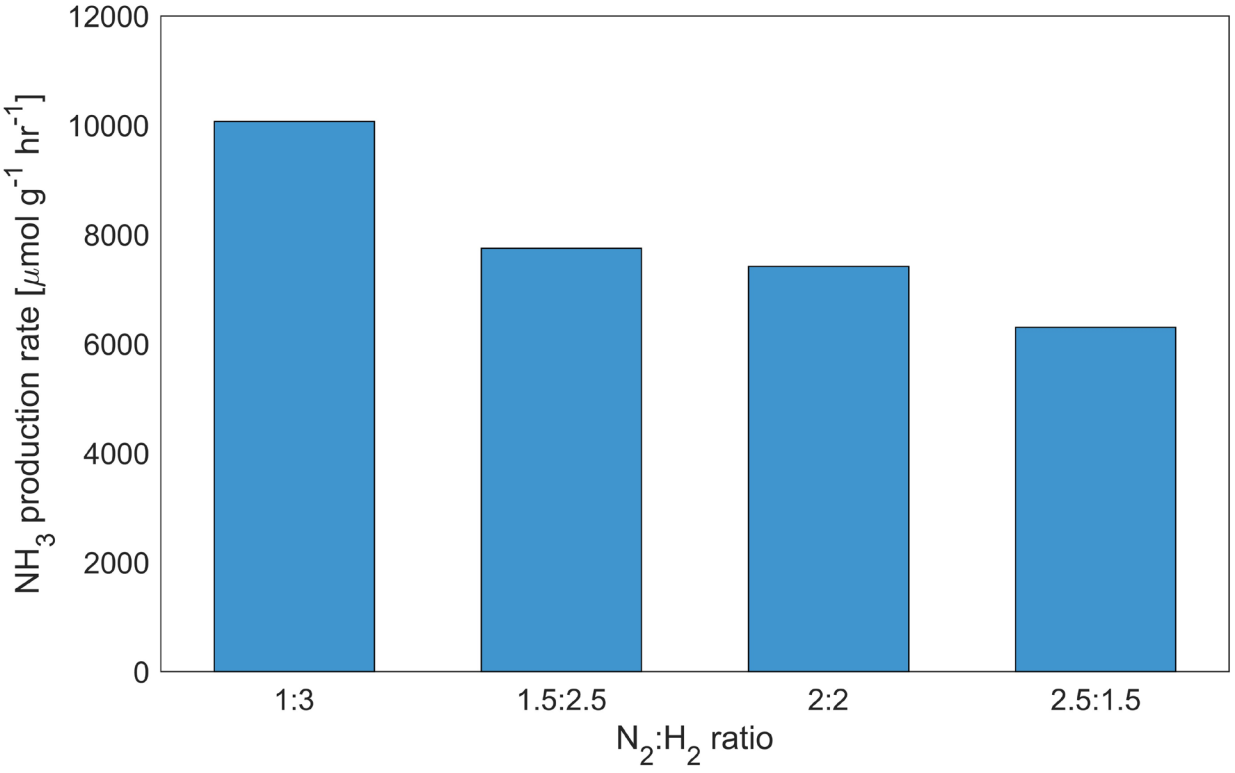


**Supplementary Fig. 9**. Effect of the $N_2/H_2$ feed mixture composition on the ammonia production rate at 400 ºC and 4 bar.

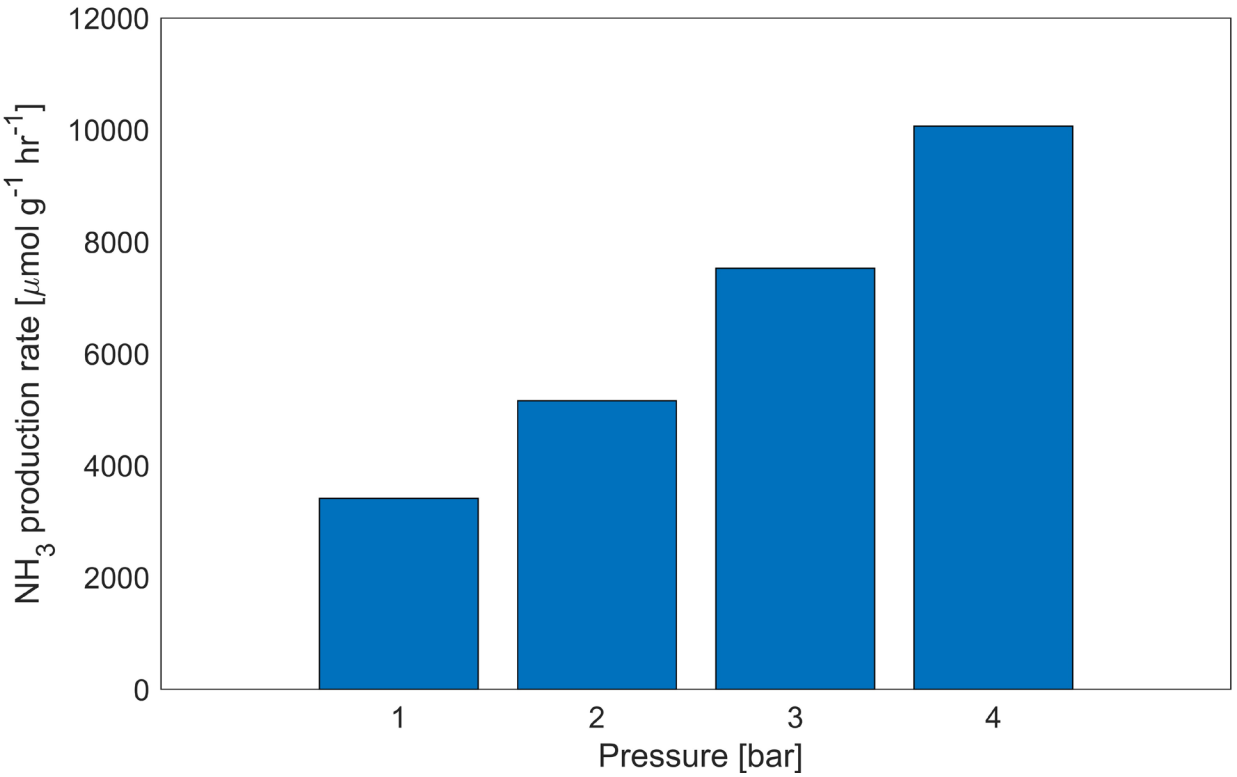


**Supplementary Fig. 10**. Ammonia production rate over the Cu-Ga catalyst at different pressures, showcasing the increase in the production rate at higher pressures at 400 ºC.

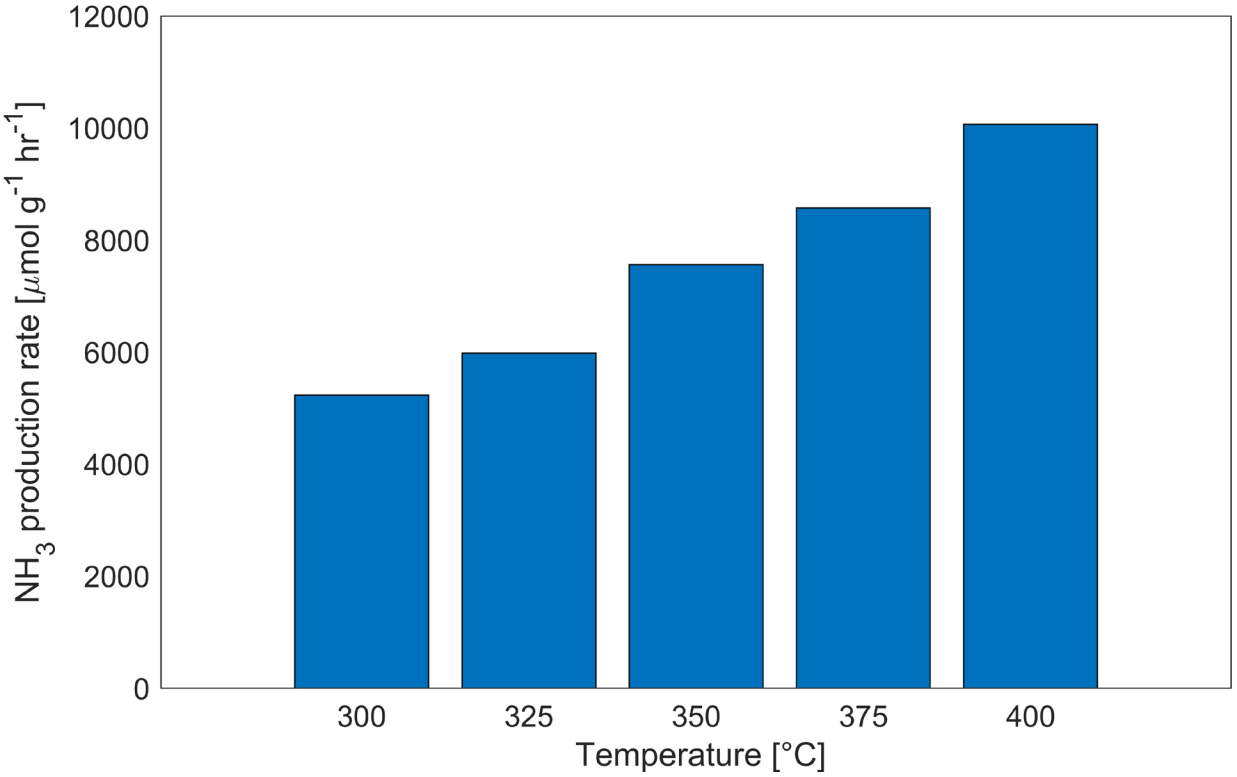


**Supplementary Fig. 11.** Ammonia production rate at different temperatures, showcasing the increase in ammonia formation over the Cu-Ga liquid metal catalyst as the reaction temperature is increased.

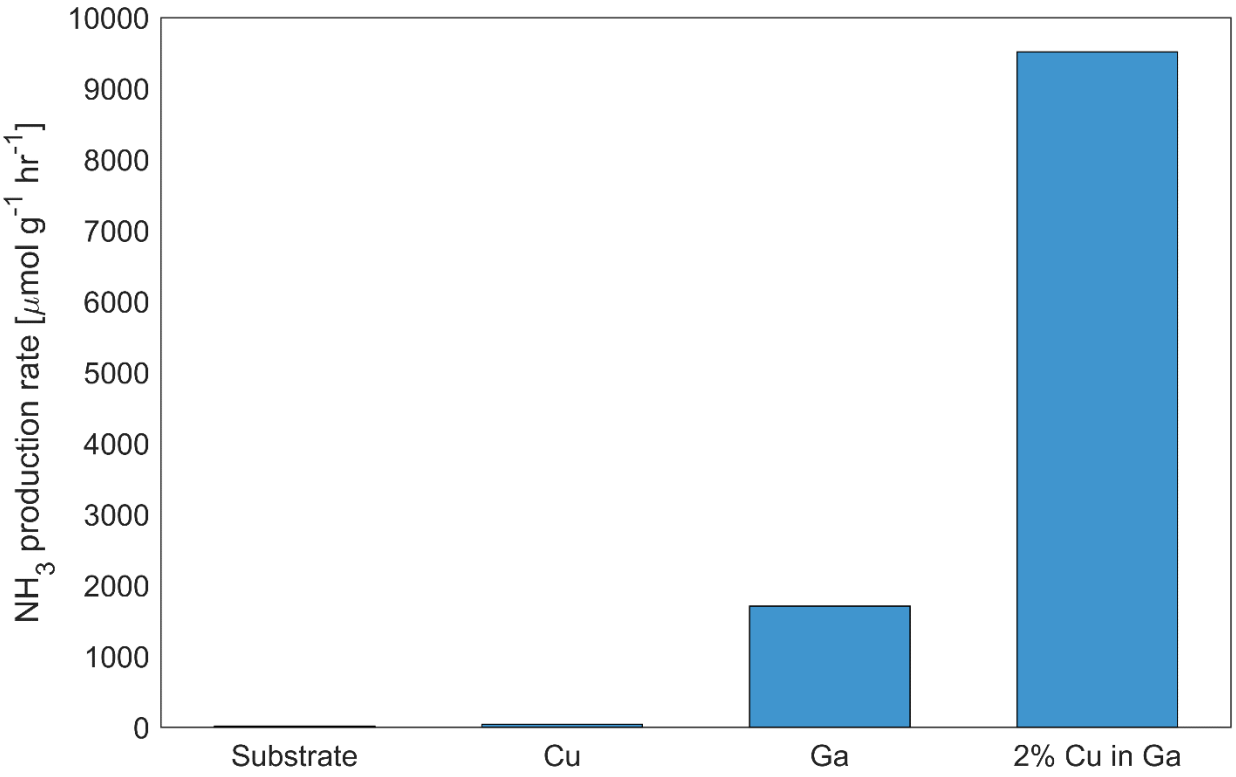


**Supplementary Fig. 12.** Comparison of the ammonia production rate obtained at 400 °C and 4 bar over the Cu-Ga liquid metal catalyst, its elemental metal constituents (Cu and Ga), and the blank inert substrate.

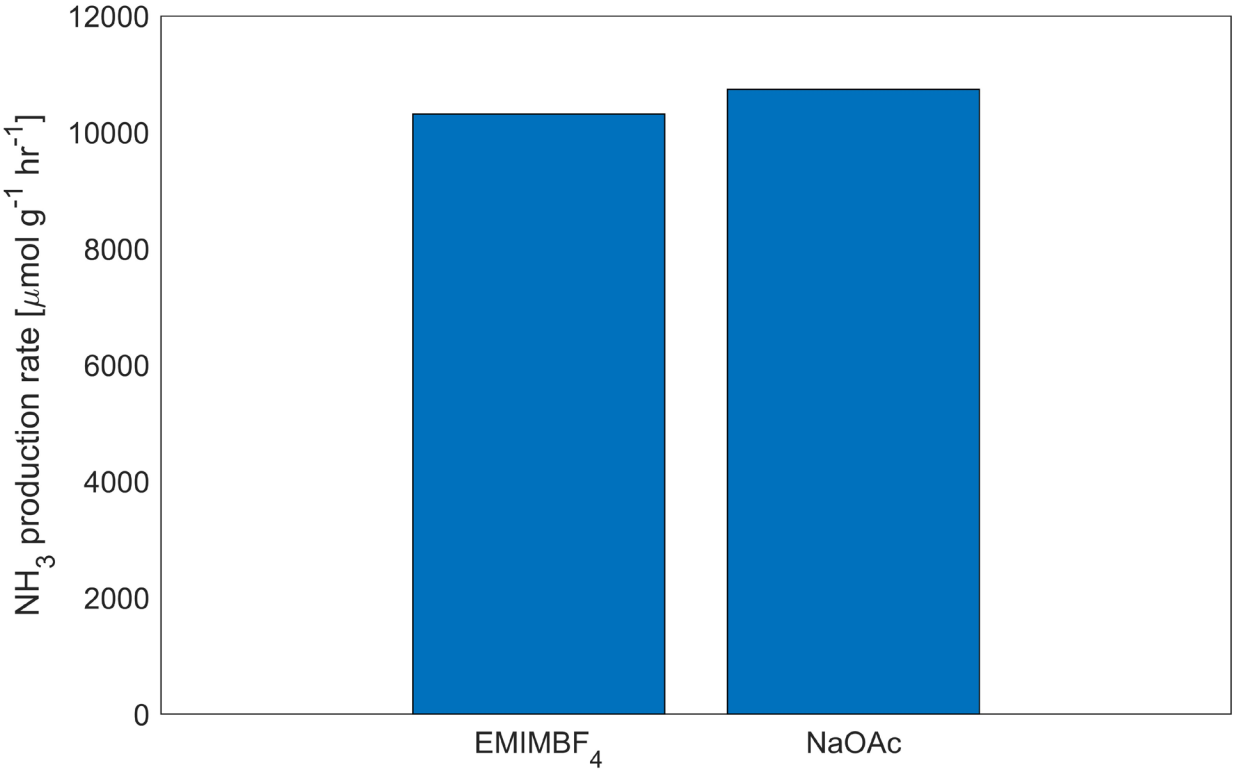


**Supplementary Fig. 13**. Comparison of the ammonia production rate obtained using Cu-Ga catalyst synthesized using different high-melting solvents.

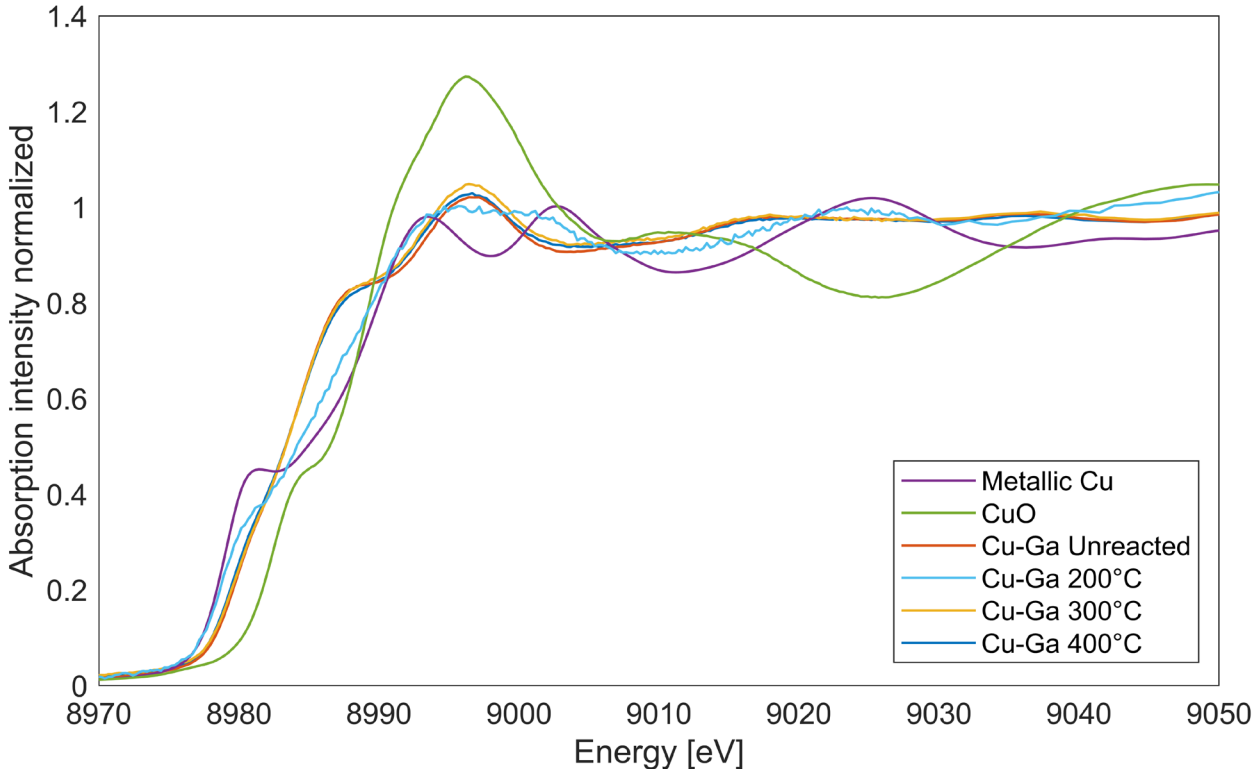


**Supplementary Fig. 14.** Cu K–edge XANES of the Cu-Ga catalyst collected at room temperature but *post reactions* at room temperature, 200 °C, 300 °C, and 400 °C.

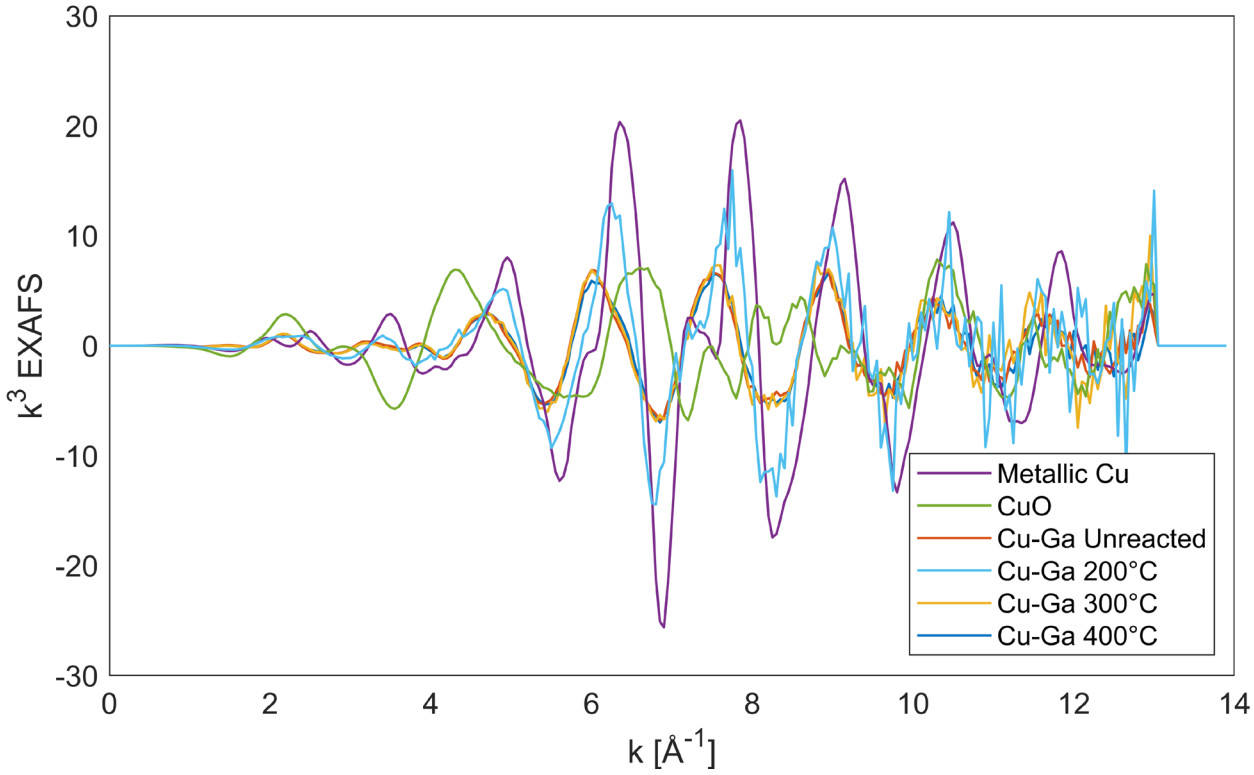


**Supplementary Fig. 15.** Cu K–edge EXAFS of the Cu-Ga catalyst post reaction at room temperature, 200 °C, 300 °C, and 400 °C.

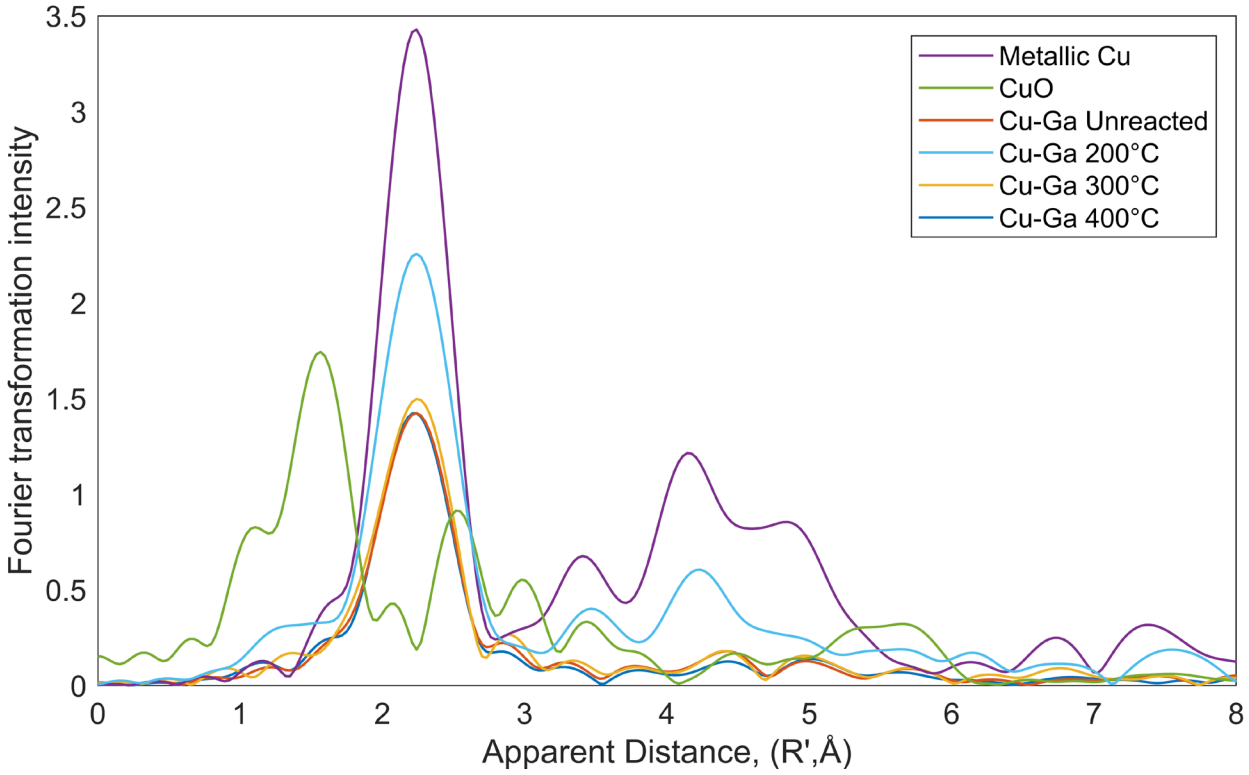


**Supplementary Fig. 16.** Cu K–edge FT of the Cu-Ga catalyst post reaction at room temperature, 200 °C, 300 °C, and 400 °C.

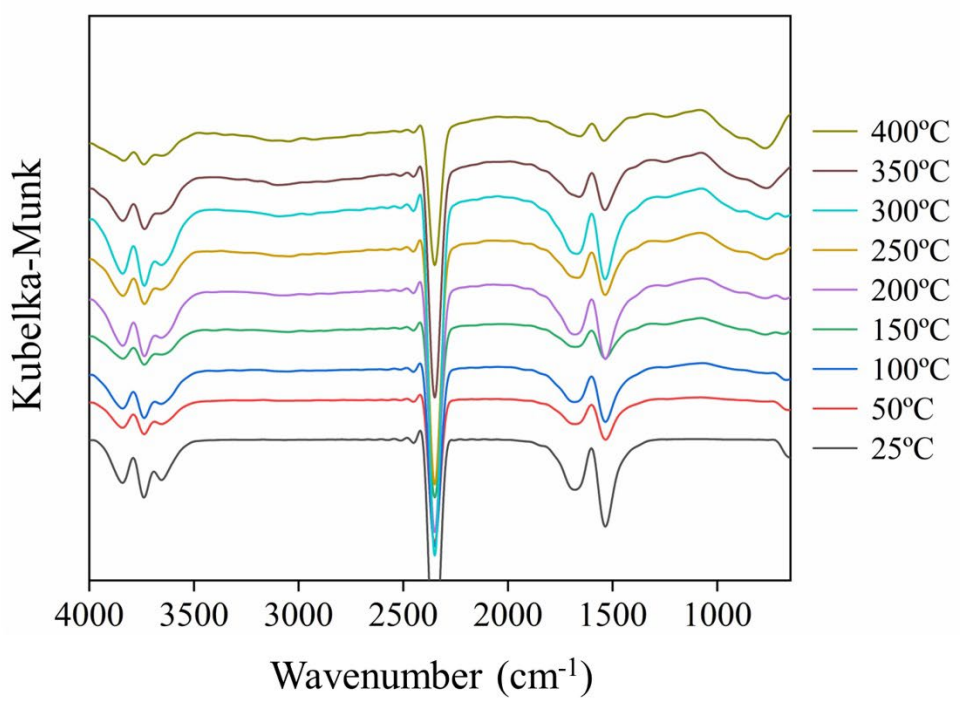


**Supplementary Fig. 17.** *In-situ* DRIFTS spectra over the Cu-Ga catalyst at different reaction temperatures, whereby pure hydrogen feed was used.

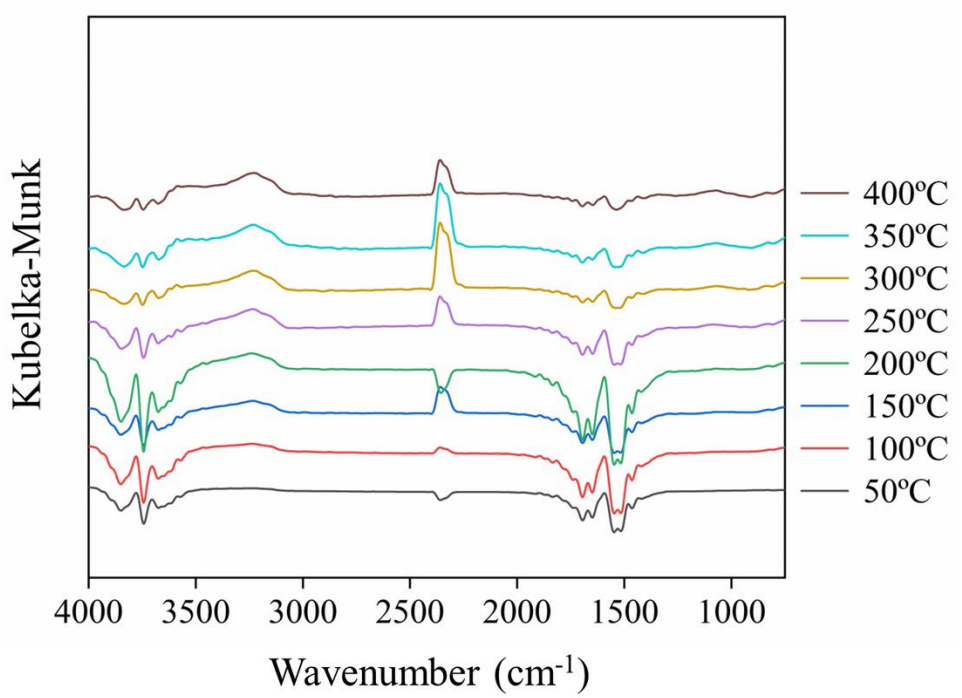


**Supplementary Fig. 18.** *In-situ* DRIFTS spectra of ammonia synthesis over pure Ga, showcasing the formation of $NH_3$ at different reaction temperatures.

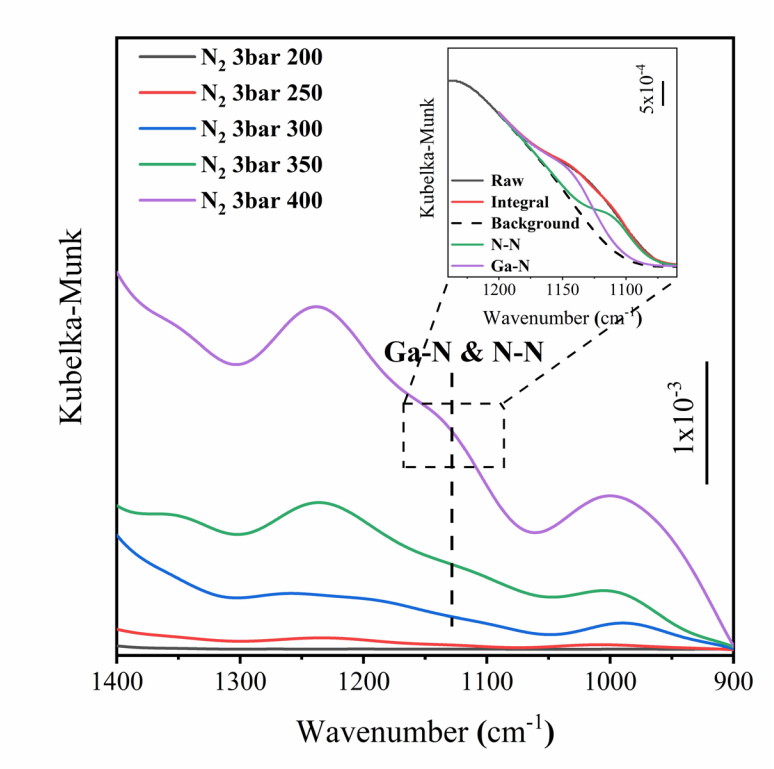


**Supplementary Fig. 19.** *In-situ* DRIFTS analysis of the Cu-Ga catalyst under $N_2$ flow at 3 bar.

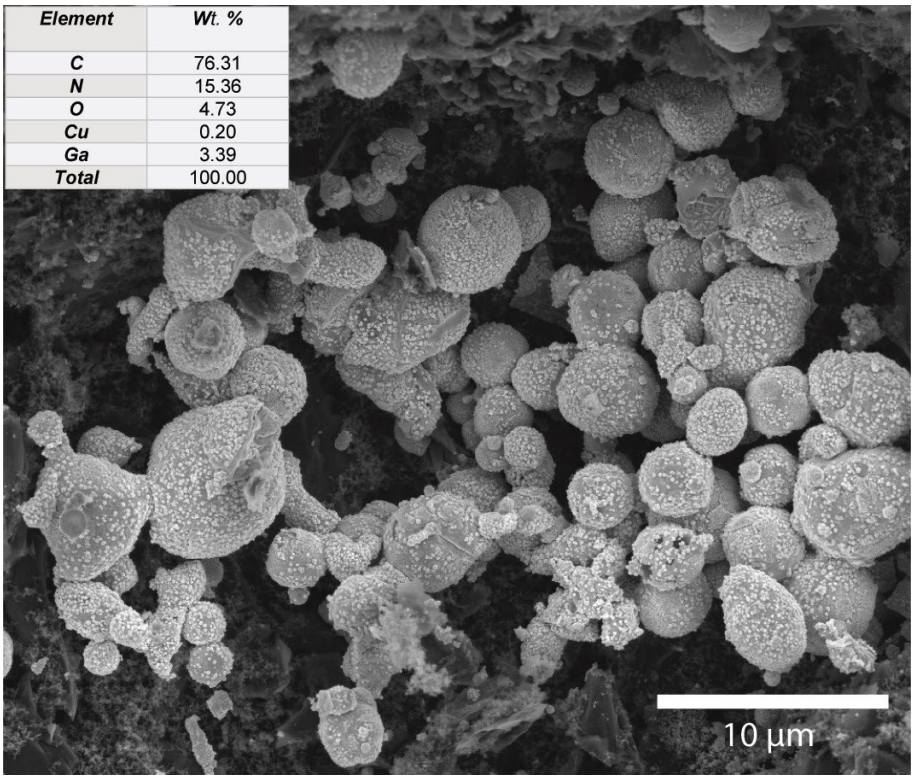


**Supplementary Fig. 20.** SEM image of the Cu-Ga catalyst after ammonia synthesis, reacted at 400 °C and 4 bar. EDX analysis (inset) was conducted as a wide area scan of the complete area encompassed in the image, showing the presence of nitrogen species post reaction.

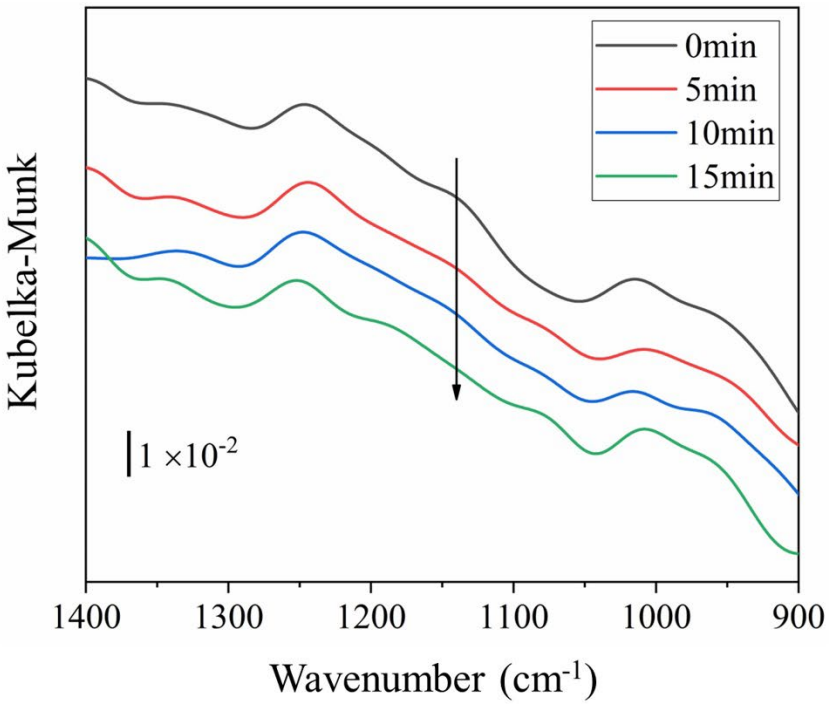


**Supplementary Fig. 21.** *In-situ* DRIFTS analysis of the nitrogen pretreated Cu-Ga catalyst under $H_2$ flow over time.

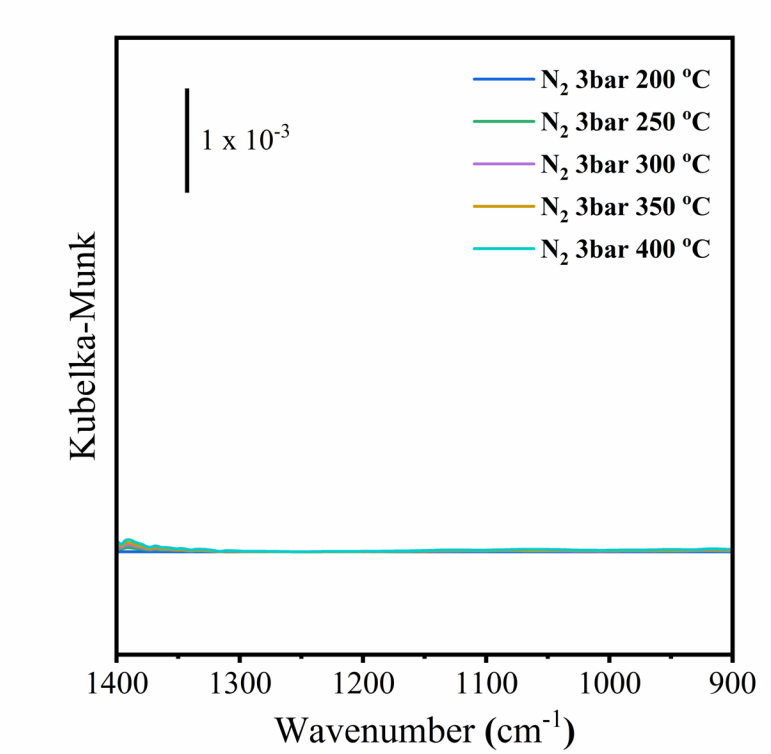


**Supplementary Fig. 22.** *In-situ* DRIFTS analysis of the pure Ga catalyst under $N_2$ flow at 3 bar.

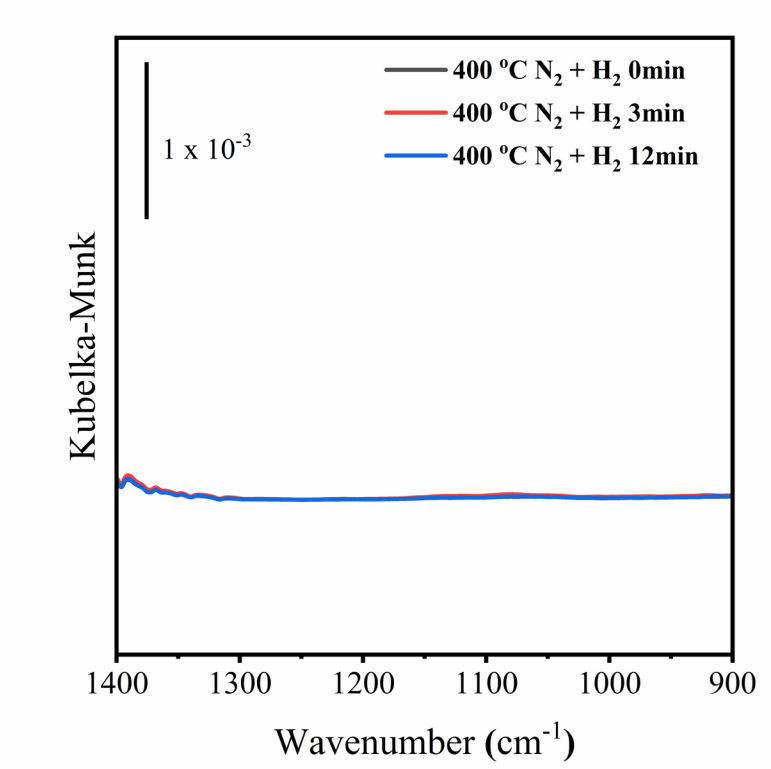


**Supplementary Fig. 23.** *In-situ* DRIFTS analysis of the nitrogen pretreated Ga catalyst under $H_2$ flow over time.

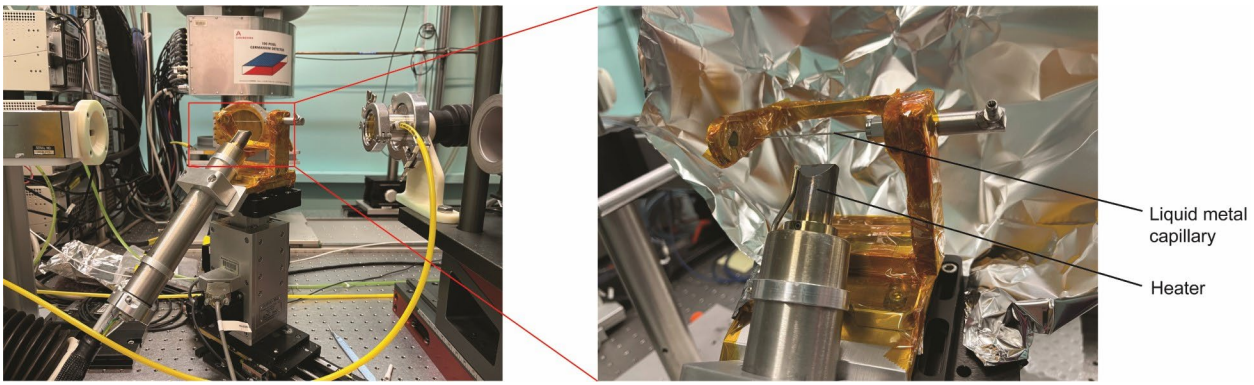


**Supplementary Fig. 24.** *In-situ* heating XAS experimental setup, comprising a capillary heater used to supply heat to the Cu-Ga alloys filled into 1 mm quartz capillaries.

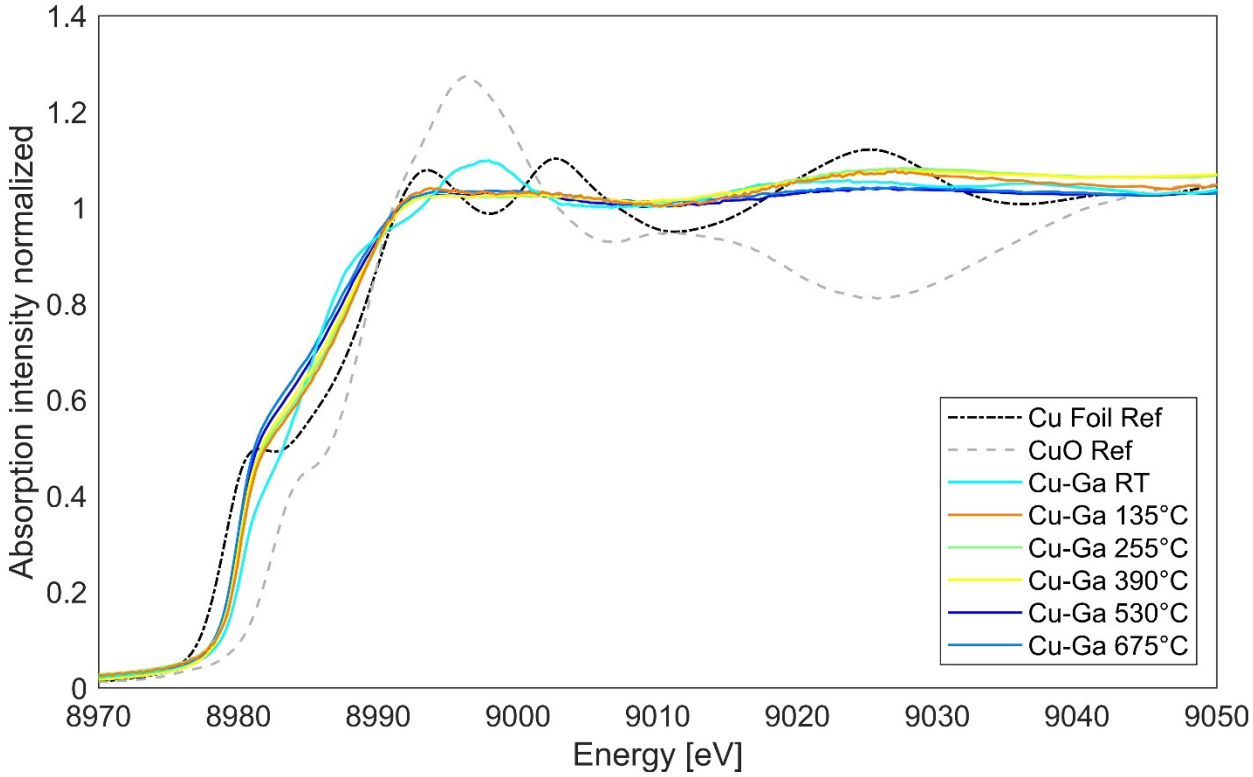


**Supplementary Fig. 25.** *In-situ* heating XANES spectra of the Cu-Ga alloy in quartz capillaries taken between room temperature and 675 °C, at the Cu K–edge.

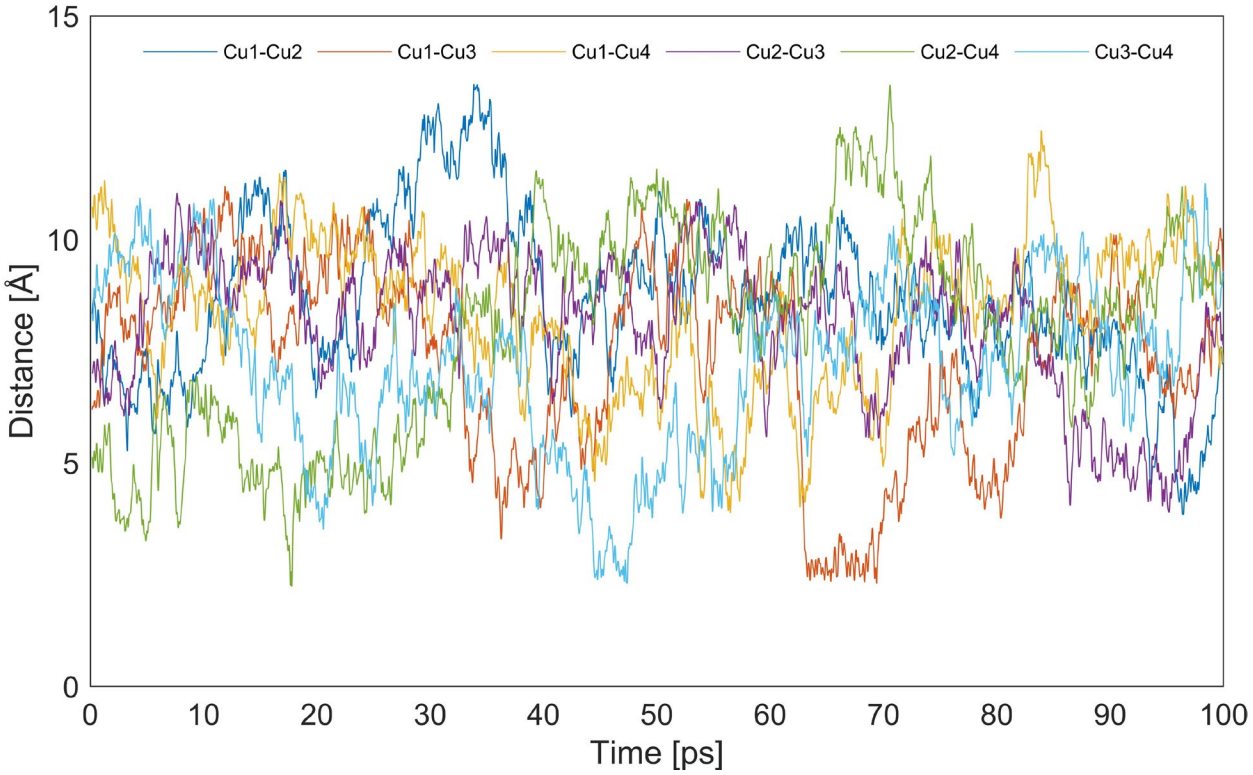


**Supplementary Fig. 26.** Cu atom pairing analysis, depicting the change in the distance between Cu atoms as a function of time in the bulk of the liquid metal from AIMD simulations at 400 °C.

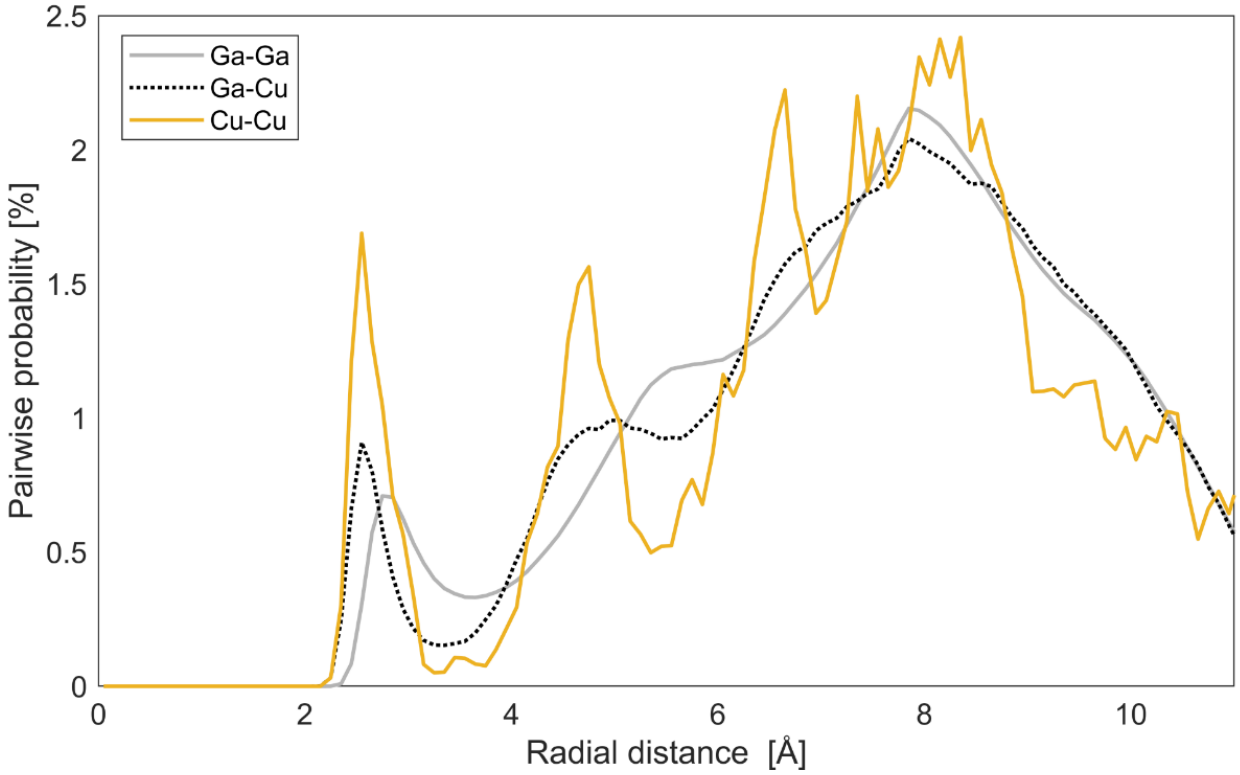


**Supplementary Fig. 27.** Atomic pairwise probability distribution in the bulk at 200 ºC from AIMD simulations.

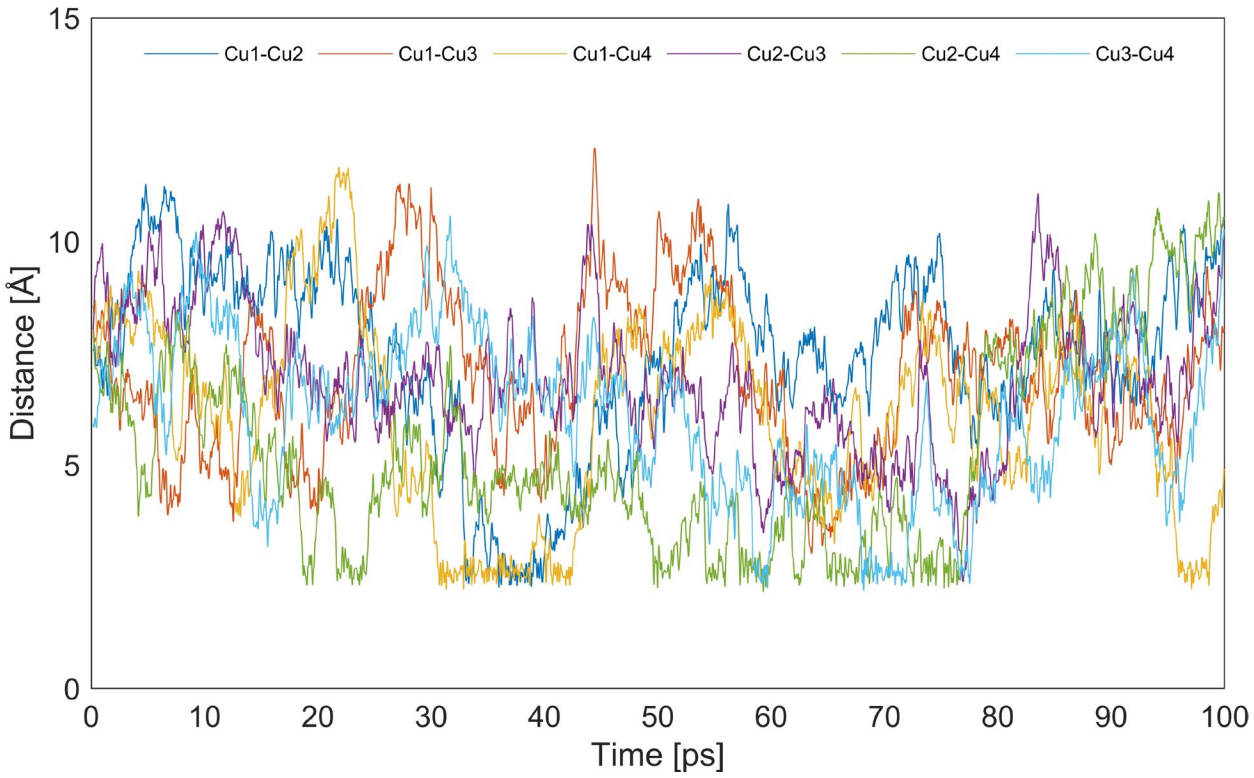


**Supplementary Fig. 28.** Cu atom pairing analysis, depicting the change in the distance between Cu atoms as a function of time across the liquid metal interface from AIMD simulations at 400 °C.

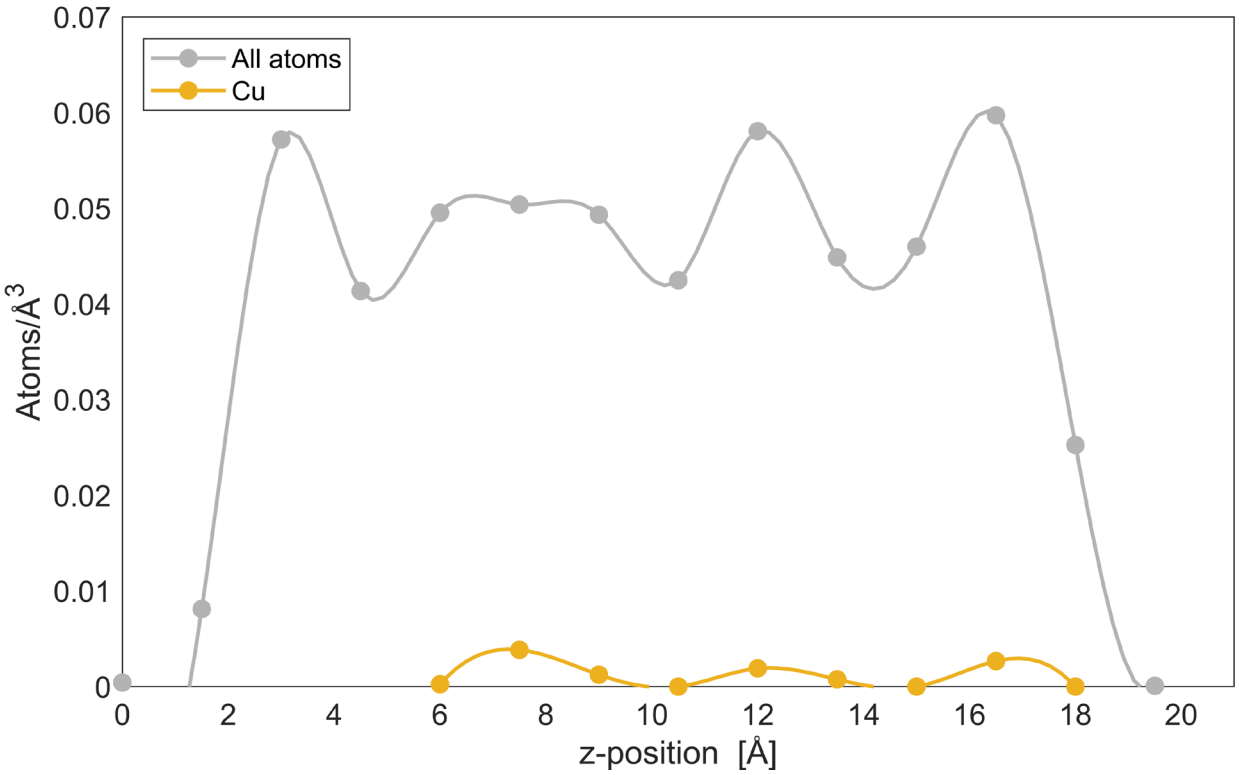


**Supplementary Fig. 29.** Atomic density profiles for all atoms and for Cu atoms as a function of z-position in the interfacial system from AIMD simulations at 400 °C.

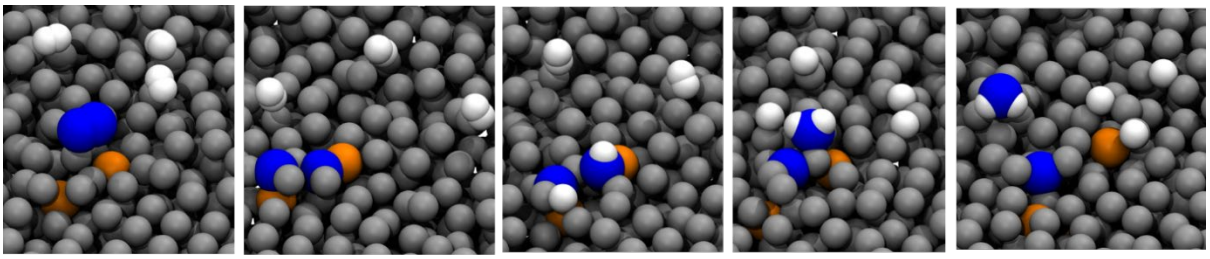


**Supplementary Fig. 30.** AIMD simulation snapshots of each step in the catalytic reaction, with relative energies in eV.

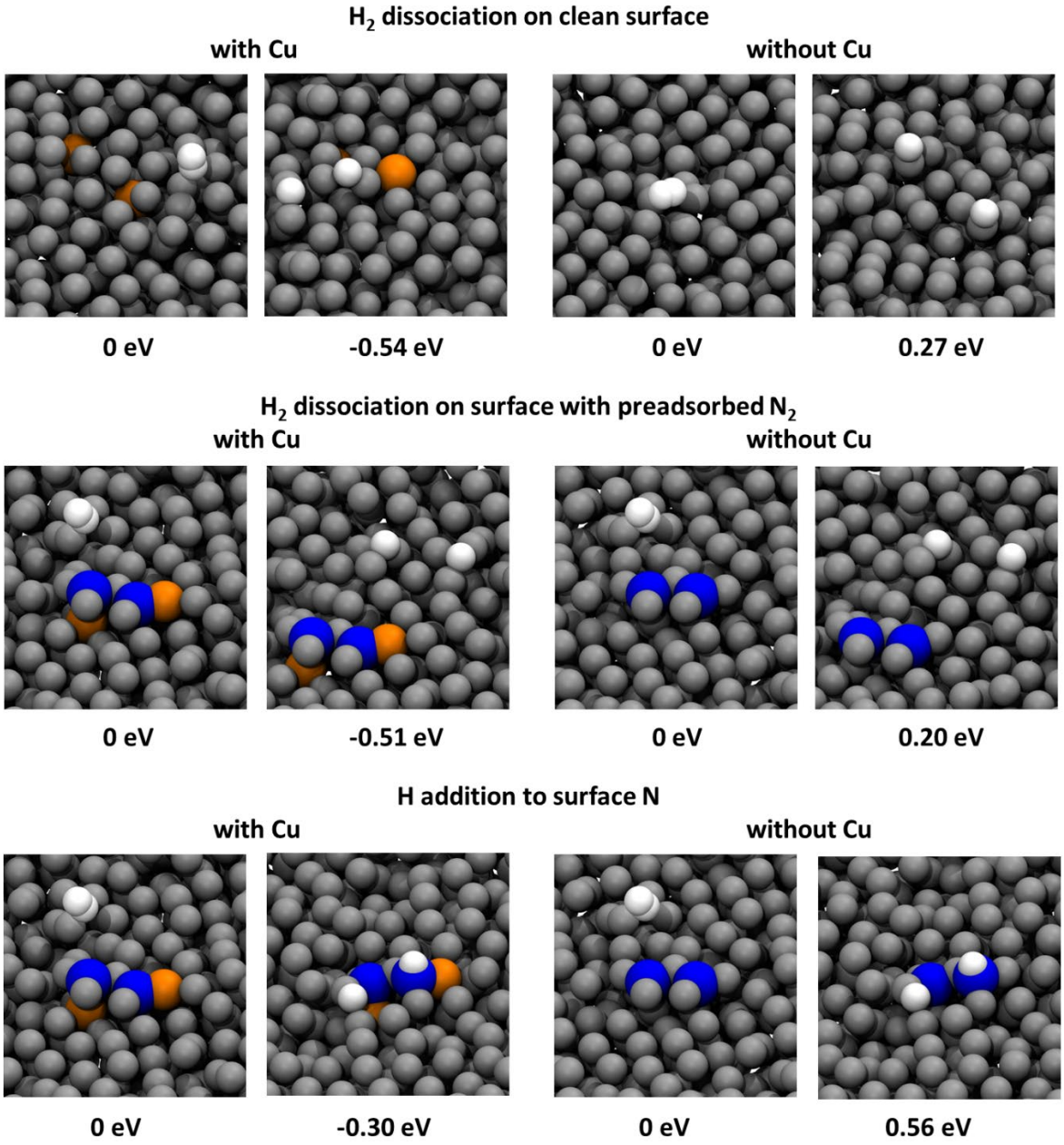


**Supplementary Fig. 31.** Reaction of $H_2$ with the surface in the presence and absence of Cu and N, showing relative energies in eV.

**Supplementary Table 2.** AIMD relative energies at the different reaction steps, highlighting the difference between the Cu-Ga catalyst and pure Ga.

| **Step** | **Energy relative to reactants With Cu (eV)** | **Energy relative to previous step With Cu (eV)** | **Energy relative to reactants No Cu (eV)** | **Energy relative to previous step No Cu (eV)** |
|---|---|---|---|---|
| Step 0 (Reactants) | 0 | 0 | 0 | 0 |
| Step 1 | -1.47 | -1.47 | -2.58 | -2.58 |
| Step 2 | -1.77 | -0.30 | -2.11 | +0.44 |
| Step 3 | -1.99 | -0.22 | -1.98 | +0.13 |
| Step 4 (Products) | -2.22 | -0.23 | -1.92 | +0.06 |

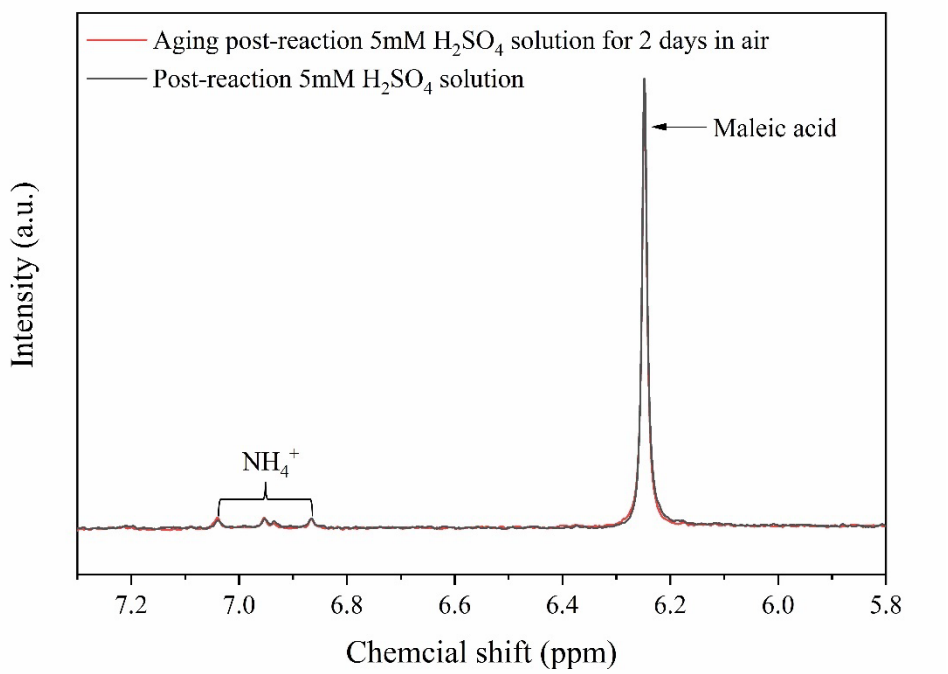


**Supplementary Fig. 32.** NMR analysis of ammonium in control experiments when pure $N_2$ is fed into the catalytic system. Negligible ammonium peaks compared to maleic acid peaks (lower than detection limits) were observed, indicating no ammonia formation in the control experiments.

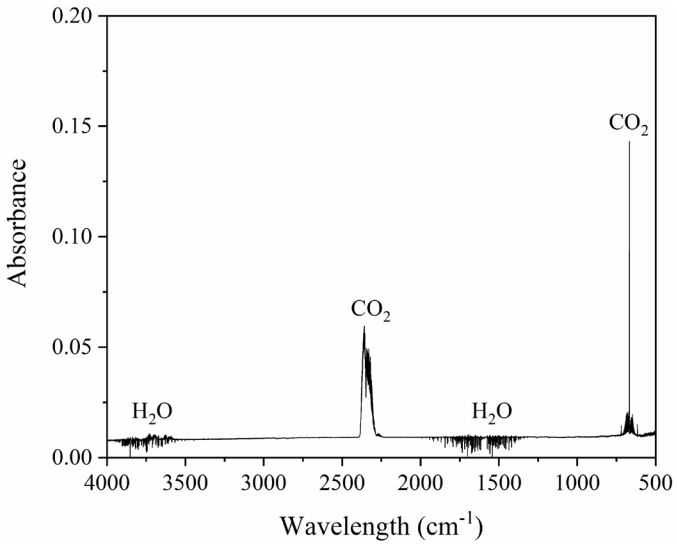


**Supplementary Fig. 33.** FTIR spectrum of gases in the $N_2$ gas cylinder, using He gas as a blank spectrum.

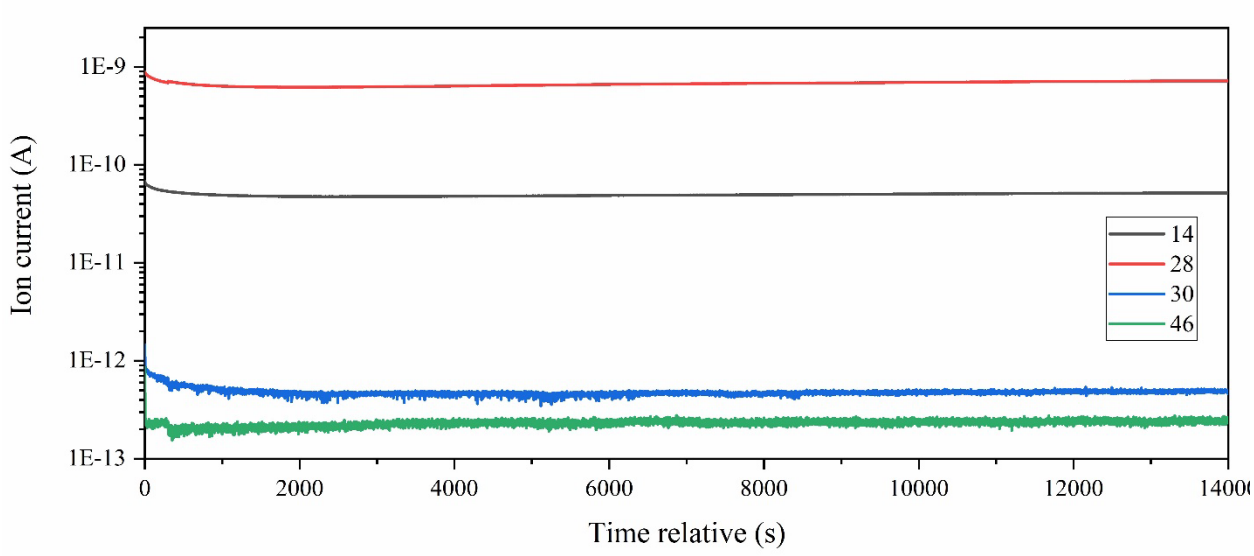


**Supplementary Fig. 34.** Detection of N (N-14), $N_2$ ($N_2$-28). NO (NO-30), and $NO_2$ ($NO_2$-46) in the reactant $N_2$ gas cylinder (>99.999%) according to mass spectroscopic responses as a function of time. The measurement is conducted with an $N_2$ flowrate of 5 ml/min.

## Supplementary References

1. Li, J.B. et al. A thermodynamic assessment of the copper–gallium system. *Calphad* **32**, 447-453 (2008).